Preprints of the 18th IFAC World Congress
Milano (Italy) August 28 - September 2, 2011

Optimal control of multidimensional population balance systems for crystal shape manipulation

N. Bajcinca [*,***] **H. A. Menarin** [*] **S. Hofmann** [**]

[*] *Max-Planck Institute for Dynamics of Complex Technical Systems, Magdeburg, Germany*
[**] *Technische Universität Berlin, Berlin, Germany*
[***] *Corresponding address: bajcinca@mpi-magdeburg.mpg.de*

Abstract: Optimal control of multidimensional particulate processes for crystal shape manipulation based on the minimum principle and the method of characteristics is discussed. The posed optimal control problems consist in achieving a desired morphology for a seed crystal population within a free or a limited time scope, while minimizing the net mass of the nucleated crystal particles. An ODE system is obtained by neglecting the natural feedback of the nucleation mass into the crystallization kinetics. Optimal solutions resulting thereof reduce to boundary value problems in only one or two unknown parameters. Moreover, for the original optimal control problem, involving the full process dynamics, a simple feasible sub-optimal solution and an upper bound for the cost function are proposed. The proposed computational approach is compared with dynamic optimization techniques in terms of the efficiency and accuracy by means of a numerical example.

Keywords: Crystal shape manipulation, multidimensional particulate systems, optimal control, minimum principle, batch crystallization

1. INTRODUCTION

Crystal shape manipulation is a critical engineering and economical venture in numerous industries, including the chemical, pharmaceutical, microelectronics, and food industry, Charpentier [2009]. Specific instances can be found in a wide scale ranging from several nm in catalysis and materials engineering, tens of μm in active pharmaceutical substances, up to several mm in base chemicals. The impact of the crystal particle shape into the product quality is likewise of key importance. For instance, it has been shown that the catalytic activity of nanocrystal particles is strongly linked to their shape, Yang et al. [2008].

From the engineering point of view, manipulation of the crystal morphology is, therefore, essential. While much of the effort in the past has gone into the control and optimization of (1D) crystal-size-distributions, see *e.g.* Braatz and Hasebe [2002], and the references therein, research on multidimensional crystallization processes has been scarce, despite of its evident importance in practice, Bajcinca et al. [2010]. The limitation in monitoring of crystal shape has been recognized as the major bottleneck, Patience and Rawlings [2001]. However, recent progress in image processing techniques for particle shape monitoring has been an impetus for intensification of theoretical research efforts in modeling and control of multidimensional crystallization processes, in general. In contrast to the traditional techniques, that utilize chemical additives for blocking or promoting of specific crystal faces, here, shape manipulation by means of temperature control only is considered.

The research on optimal control of crystallization processes has been extensive ever since it was first addressed in Mullin and Nyvlt [1971], where the authors realized that the final crystal size can be increased by using a "programmed" crystallization temperature trajectory rather than the natural cooling of the solution. Thereafter, diverse optimal control problems were formulated and solved using optimal control theory and numerical methods, including Jones [1974], Ajinkya and Ray [1974], Miller and Rawlings [1994], Lang et al. [1999], and many other. One of the rare works which deals with optimization of multidimensional processes is Ma et al. [2002], where a sequential quadratic programming (SQP) algorithm was used for maximizing the average length of crystals. Diverse optimal control solutions for shape manipulation of single crystal particles are discussed in Bajcinca et al. [2010] and Bajcinca et al. [2011]. Other relevant references for the ideas presented in this article are the recent works Hofmann and Raisch [2010] and Bajcinca and Hofmann [2011], where the minimum principle is applied for the design of efficient optimization algorithms for size-independent and size-dependent growth rate kinetics, respectively.

This work considers optimization of a multidimensional batch crystallization process with a special emphasis on the shape manipulation for crystal population systems. The optimization task we refer to consists in suppressing the nucleation, while steering the growth of the seed crystals towards the required final shape. To this end, we use the method of characteristics to derive a model from the population balance equation with a source and advective term in Section 2. The optimization problem in

two scenarios is formulated and its solutions using the minimum principle are given in Section 3. Thereby, a model reduction is introduced by removing the natural feedback of the nucleated crystal mass into the crystallization kinetics. The obtained solutions result from two boundary value problems with one and two unknown parameters, respectively. Finally, in Section 4, a numerical example taken from the literature is worked out to compare the efficiency and accuracy of our optimization scheme with standard dynamic optimization ones.

2. MULTIDIMENSIONAL PARTICULATE SYSTEMS

A large class of particulate systems are conveniently modeled by an advective linear first-order partial differential equation (PDE), referred to as the population balance equation (PBE), which expresses the conservation of the number of particles in an infinitesimal volume element of the state space (a subset of $\mathbb{R}^n_{\geq 0}$)

$$\frac{\partial f}{\partial t} + \sum_{i=1}^{n} G_i(t) \frac{\partial f}{\partial L_n} = B(t) \prod_{i=1}^{n} \delta(L_i), \ t > 0, \tag{1a}$$

$$f(L_1, \ldots, L_n, 0) = f_{\text{seed}}(L_1, \ldots, L_n). \tag{1b}$$

The function $f(L_1, \ldots, L_n, t)$ represents the population density function (PDF), defined as the number density of particles per unit volume, *i.e.* the net number of particles is then given by $\int_0^\infty \ldots \int_0^\infty f(L_1, \ldots, L_n, t) \mathrm{d}L_1 \ldots \mathrm{d}L_n$. The function $f_{\text{seed}}(L_1, \ldots, L_n)$ stands for the given initial density function. The advective term $G_i = \partial L_i / \partial t$ refers to the i-th component of the growth rate vector of a particle in the state space, which is here assumed to be size independent. In the source term, in the right-hand side of (1a), $B(t)$ stands for the nucleation (or birthrate) function, and $\delta(L_i)$ is the Dirac function, suggesting that new particle nuclei are born at negligible size. Other phenomena, such as the particle agglomeration and breakage, are ignored.

2.1 Method of characteristics

The method of characteristics is a standard technique for solving general first order of PDEs by transforming them into a family of ODEs parametrized by given initial conditions on a suitable hypersurface. For the sake of completeness, we review here very briefly the method, which we use for the solution of (1a)-(1b).

Consider a linear first order PDE in the form

$$F(x_1, \ldots, x_n) \cdot \nabla f(x_1, \ldots, x_n) = \phi(x_1, \ldots, x_n), \tag{2a}$$

where $f : \mathbb{R}^n \to \mathbb{R}$ is the function to be solved for, $F : \mathbb{R}^n \to \mathbb{R}^n$ is a vector field, and $\phi : \mathbb{R}^n \to \mathbb{R}$. Then, if f is a solution for the equation (2a), we have that

$$(F_1, \ldots, F_n, \phi) \cdot (f_{x_1}, \ldots, f_{x_n}, -1) = 0, \tag{2b}$$

where F_i and f_{x_i} are the components of F and ∇f, respectively. If S is the graph of f, defined by

$$S = (x_1, \ldots, x_n, z)$$

with $z = f(x_1, \ldots, x_n)$, the equation (2b) suggests that the vector $(F_1, \ldots, F_n, \phi)$ lies in the tangent plane to S at $(x_1, \ldots, x_n, z)$, because $(f_1, \ldots, f_n, -1)$ is perpendicular to S. Thus, to find a solution, one should construct a surface S, such that at each its point $(x_1, \ldots, x_n, z)$, the vector $(F_1, \ldots, F_n, \phi)$ lies in the tangent plane. To this end, note that curves $\mathcal{C} = (x_1(\beta), \ldots, x_n(\beta), z(\beta))$ on S exist, such that

$$\frac{\mathrm{d}x_i}{\mathrm{d}\beta} = F_i(x_1(\beta), \ldots, x_n(\beta)), \quad i = 1, \ldots, n$$

$$\frac{\mathrm{d}z}{\mathrm{d}\beta} = \phi(x_1(\beta), \ldots, x_n(\beta)). \tag{2c}$$

This system of ODEs can be seen as the tool for constructing particular curves $\mathcal{C}$ on S, known as the integral curves for the vector field $(F_1, \cdots, F_n, \phi)$, or characteristic curves (shortly, also characteristics) of the PDE (2a), which result by solving (2c) for $x_i = x_i(\beta)$ and $z = z(\beta)$. The union of integral curves $\mathcal{C}$ defines the integral surface S for $(F_1, \cdots, F_n, \phi)$, which represents the required solution $z = f(x_1, \ldots, x_n)$ for the PDE (2a).

Obviously, such constructed solutions are not unique. Typically, the PDE (2a) is associated with some restriction or boundary condition on Γ

$$f|_\Gamma = \phi, \tag{2d}$$

where Γ is a given (noncharacteristic) manifold in $\mathbb{R}^{n-1}$, parametrized by

$$(\gamma_1(r_1, \ldots, r_{n-1}), \ldots, \gamma_n(r_1, \ldots, r_{n-1})). \tag{2e}$$

Intuitively, one needs to select the integral surfaces which contain the manifold Γ, that is the characteristics that emanate from the manifold Γ at $\beta = 0$. In other words, the ODE system (2c) are associated the boundary conditions

$$x_i(r_1, \ldots, r_{n-1}, 0) = \gamma_i(r_1, \ldots, r_{n-1}), \ i = 1, \ldots, n$$
$$z(r_1, \ldots, r_{n-1}, 0) = \phi(r_1, \ldots, r_{n-1}). \tag{2f}$$

whose solutions are, say

$$x_i = x_i(r_1, \ldots, r_{n-1}, \beta), \quad i = 1, \ldots, n.$$
$$z = z(r_1, \ldots, r_{n-1}, \beta). \tag{2g}$$

As Γ is assumed to be noncharacteristic, the first n equations can be uniquely inverted, *i.e.*

$$\beta = \beta(x_1, \ldots, x_n), \ r_i = r_i(x_1, \ldots, x_n), \ i = 1, \ldots, n-1,$$

which are now substituted into (2f), to end up with the sought integral surface $z = f(x_1, \ldots, x_n)$.

2.2 PBE solution

Consider the homogeneous equation corresponding to (1a). Physically, nucleation is set to zero, while the resulting homogenous PDF solution refers to the crystal seeds, which we denote by f_{s}, and require it to satisfy the full initial conditions (1b)

$$\frac{\partial f_{\text{s}}}{\partial t}(L_1, \ldots, L_n, t) + \sum_{i=1}^{n} G_i(t) \frac{\partial f_{\text{s}}}{\partial L_i}(L_1, \ldots, L_n, t) = 0 \tag{3}$$

$$f_{\text{s}}(L_1, \ldots, L_n, 0) = f_{\text{seed}}(L_1, \ldots, L_n). \tag{4}$$

Applying the concepts from Section 2.1, we will construct characteristic curves $\mathcal{C} = (t, L_1, \ldots, L_n, z)$ by using a parametrization $(\beta, r_1, \ldots, r_n)$. The curve $\mathcal{C}$ with $z = f_{\text{s}}(t, L_1, \ldots, L_n)$, then, lies on the graph of the solution, while the parametrization $(r_1, \ldots, r_n, \beta) \mapsto (L_1, \ldots, L_n, t)$ needs to be inverted to get the solution. From (2c)

$$\frac{dt}{d\beta} = 1, \quad \frac{dL_i}{d\beta} = G_i(\beta), \quad \frac{dz}{d\beta} = 0. \tag{5}$$

Restricting the solution of the system of ODEs (5) to match the initial condition (4)

$$t(r_1, \ldots, r_n, 0) = 0,$$
$$L_i(r_1, \ldots, r_n, 0) = r_i, \quad i = 1, \ldots, n$$
$$z(r_1, \ldots, r_n, 0) = f_{\text{seed}}(r_1, \ldots, r_n),$$

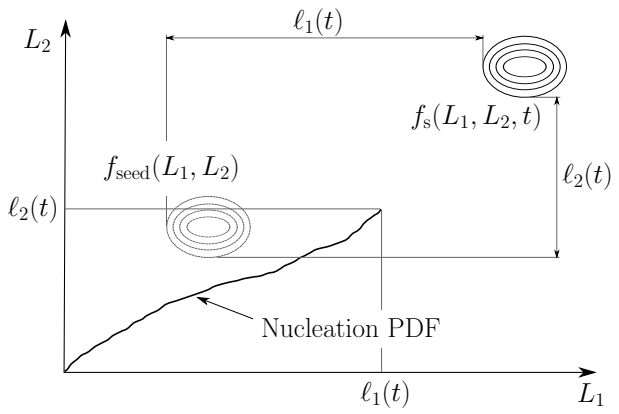

Fig. 1. Bidimensional PBE solution at a time instant t.

we obtain the characteristic curves parametrized in terms of $(r_1, \ldots, r_n, \beta)$

$$t(r_1, \ldots, r_n, \beta) = \beta,$$
$$L_i(r_1, \ldots, r_n, \beta) = r_i + \int_0^\beta G_i(\xi)d\xi,\ i = 1, \ldots, n,$$
$$z(r_1, \ldots, r_n, \beta) = f_{\rm seed}(r_1, \ldots, r_n).$$

Inverting the mapping $(r_1, \ldots, r_n, \beta) \mapsto (L_1, \ldots, L_n, t)$,

$$r_i = L_i - \ell_i(t), \quad \ell_i(t) := \int_0^t G_i(\xi)d\xi,\ i = 1, \ldots, n. \quad (6)$$

Hence, the homogenous solution reads

$$f_{\rm s}(L_1, \ldots, L_n, t) = f_{\rm seed}(L_1 - \ell_1(t), \ldots, L_n - \ell_n(t)), \quad (7)$$

that is, this solution is a translation of the initial PDF, as a consequence of the growth of the crystals, see Fig. 1.

Now, let $f_{\rm n}$ be the particular solution of the PBE, which satisfies the homogenous initial condition $f_{\rm n}(L_1, \ldots, L_n, 0) = 0$. The ODE system in (5) preserves the same directions for the characteristic curves, except for the z dimension

$$\frac{dz}{d\beta}(r_1, \ldots, r_n, \beta) = B(\beta)\prod_{i=1}^n \delta(L_i),\ z(r_1, \ldots, r_n, 0) = 0,$$

implying

$$z(r_1, \ldots, r_n, \beta) = \int_0^\beta B(\xi)\prod_{i=1}^n \delta(r_i + \ell_i(\xi))d\xi. \quad (8)$$

Thus, the particular solution, referring to the nucelation PDF is given by

$$f_{\rm n}(L_1, \ldots, L_n, t) = \int_0^t B(\xi)\prod_{i=1}^n \delta(L_i - \ell_i(t) + \ell_i(\xi))d\xi. \quad (9)$$

To conclude, while the initial distribution is translated, the nucleated PDF emerges over a line domain, because of the Dirac distribution inside the integral (9). This is depicted in Fig. 1. Note that (7) and (9) reflect a decomposition of the total density function into two separate parts referring to the seed and nucleation crystals, respectively.

2.3 Volume computation

With reference to the crystallization process dynamics, which we will shortly focus on, for our computation framework the net volume function $V_C = V_C(t)$ of the crystal particles is essential. Given the expression for the volume of a single particle $\eta = \eta(L_1, \ldots, L_n)$, and the solution for the density function $f(t, L_1, \ldots, L_n)$, the expression for the net volume reads

$$V_C(t) = \int_0^\infty \ldots \int_0^\infty f(L_1, \ldots, L_n, t)\eta(L_1, \ldots, L_n)\mathrm{d}L_1 \ldots \mathrm{d}L_n. \quad (10)$$

Let $V_{C,\rm s}$ and $V_{C,\rm n}$ be the volume components stemming from the seed $f_{\rm s}$, and the nucleation $f_{\rm s}$ distributions, respectively. Then, from (7), it follows

$$V_{C,s}(t) = \int_0^\infty \ldots \int_0^\infty f_{\rm seed}(L_1, \ldots, L_n) \times \times \eta\left(L_1 + \ell_1(t), \ldots, L_n + \ell_n(t)\right) dL_1 \ldots dL_n \quad (11)$$

and

$$V_{C,n}(t) = \int_0^t \int_0^\infty \ldots \int_0^\infty B(\xi)\prod_{i=1}^n \delta(L_i - \ell_i(t) + \ell_i(\xi)) \eta(L_1, \ldots, L_n)dL_1 \ldots dL_n d\xi = \int_0^t B(\xi)\eta(\ell_1(t) - \ell_1(\xi), \ldots, \ell_n(t) - \ell_n(\xi))d\xi, \quad (12)$$

which is a line integral along the time-parameterized trajectory $(\ell_1(t), \ldots, \ell_n(t))$.

2.4 Bidimensional crystallization process

Bidimensional particulate crystallization systems ($n = 2$), are often encountered in practice. The corresponding population balance equations for $f(L_1, L_2, t)$ is given by

$$\frac{\partial f}{\partial t} + G_1(t)\frac{\partial f}{\partial L_1} + G_2(t)\frac{\partial f}{\partial L_2} = B(t)\delta(L_1)\delta(L_2), \quad (13)$$
$$f(L_1, L_2, 0) = f_{\rm seed}(L_1, L_2). \quad (14)$$

The growth and secondary nucleation rates depend on the relative supersaturation σ, and on the total volume of crystals according to

$$B(t) = k_b\sigma(t)^b V_C(t), \quad (15a)$$
$$G_1(t) = k_{g_1}\sigma(t)^{g_1}, \quad G_2(t) = k_{g_2}\sigma(t)^{g_2}. \quad (15b)$$

We consider here the secondary nucleation only in the metastable region, and do not address the primary nucleation. The supersaturation σ is defined by

$$\sigma(t) = \frac{c(t)}{c_{\rm sat}(t)} - 1, \quad (15c)$$

where c is the solution concentration, while the solubility $c_{\rm sat}$ is a function of the solution temperature T

$$c_{\rm sat}(t) = A_0 + A_1 T(t) + A_2 T(t)^2. \quad (15d)$$

Note that for a given function $c(t)$, (15c) and (15d) can be solved analytically for $T(t)$. Thus, $\sigma(t)$ or $T(t)$ can be used interchangeably as the control variables; here, we employ the former, while the temperature T will be considered as output (see below). Namely, its optimal profile is to be stored, and used for the control of a real process.

Finally, the mass balance describes the solute consumption. From the mass conservation of the system, the solution concentration c, in grams of solute per grams of solvent, is given by

$$c(t) = c_0 - \rho_c(V_C(t) - V_C(0)), \quad (15e)$$

where ρ_c is the mass density of crystal particles.

For a given expression of $\eta = \eta(L_1, L_2)$, representing the volume of a single particle of the underlying crystal morphology, the volume $V_{C,s}(t)$ in (11) can be explicitly expressed in terms of the evolution of the trajectory $\ell_i(t)$. To illustrate this, let $n = 2$, and consider

$$\eta(L_1, L_2) = \frac{1}{3}L_1^3 + (L_2 - L_1)L_1^2, \quad L_2 > L_1, \quad (15f)$$

which refers to the KDP crystal and will be employed in Section 4 as the case-study for a numerical example. Substitution of this into equation (11), we obtain

$$\begin{aligned} V_{C,s}(t) =& \eta(\ell_1(t),\ell_2(t))\,\mu_{00}(0) + 2\ell_1(t)(\ell_2(t)-\ell_1(t))\,\mu_{10}(0) \\ &+ (\ell_2(t)-2\ell_1(t))\mu_{20}(0) + \ell_1^2(t)\mu_{01}(0) \\ &+ 2\ell_1(t)\mu_{11}(0) + V_C(0), \end{aligned} \tag{15g}$$

where $\mu_{ij}(0)$ $(i=0,1,2,\ j=0,1)$ are constants, representing the moments of the distribution $f_{\text{seed}}(L_1,L_2)$ (see below), given by

$$\mu_{ij}(0) = \int_0^\infty \int_0^\infty f_{\text{seed}}(L_1,L_2,t) L_1^i L_2^j dL_1 dL_2. \tag{16}$$

Note that $V_{C,s}(\ell_1,\ell_2)$ in (15g) is a polynomial in terms of ℓ_1 and ℓ_2. Now we are in the position to define the integro-differential model.

Definition 1. (*Integro-differential model).* With $\sigma(t) > 0$ as input, use the process kinetics (15a)-(15b) to compute $B(t)$, $G_1(t)$ and $G_2(t)$. From (6), $\ell_1(t)$ and $\ell_2(t)$ are integrated, and hence, $L_1(t)$ and $L_2(t)$, too. Using (15g) and (12) compute the total volume $V_C(t) = V_{C,\text{s}}(t) + V_{C,\text{n}}(t)$. The, computation loop in now closed, as $V_C(t)$ is fed back to (15a) for $B(t)$. The temperature $T(t)$, which is a model output, is computed by solving the kinetics equations (15c)-(15e) for $T(t)$.

In the latter integration scheme the computation of the net volume $V_C(t)$ can be carried out by making use of the bidimensional moment model. Therefore, note that a given density function $f(L_1,L_2,t)$ can be associated the mixed moments, defined as

$$\mu_{ij}(t) = \int_0^\infty \int_0^\infty f(L_1,L_2,t) L_1^i L_2^j dL_1 dL_2. \tag{17}$$

Using this definition, the following ODE system can be derived from the PBE (13), see *e.g.* Ma et al. [2002]

$$\begin{aligned} &\dot{\mu}_{00}(t) = B(t), \\ &\dot{\mu}_{ij}(t) = iG_1(t)\mu_{i-1,j}(t) + jG_2(t)\mu_{i,j-1}(t),\ i,j>0. \end{aligned} \tag{18}$$

For a given expression $\eta(L_1,L_2)$, an expression for $V_C(t)$ in terms of mixed moments can be derived. *E.g.* for (15f)

$$V_C(t) = \mu_{21}(t) - \tfrac{2}{3}\mu_{30}(t). \tag{19}$$

In view of (15a), it is obvious that the moment model (18) is closed. This leads us to the following integration scheme.

Definition 2. (*Moment model).* Consider $\sigma(t) > 0$ as input, and use the process kinetics (15a)-(15b) to compute $B(t)$, $G_1(t)$ and $G_2(t)$. Integrate the moment model (18) for the moments $\mu_{21}(t)$ and $\mu_{30}(t)$. Then, use (19) to compute $V_C(t)$. At this point, the computation loop closes. Again, the temperature $T(t)$ is computed by solving (15c)-(15e) for T. If required, the trajectory $(\ell_1(t),\ell_2(t))$ is computed by integrating (6).

For both models, to solve for $f_{\text{n}}(L_1,L_2,t)$ and $f_{\text{s}}(L_1,L_2,t)$ of the PBE (13)-(14), use (7) and (9). [Of course, $f_{\text{seed}}(L_1,L_2)$ is available from the initial conditions.]

We assume that the operation is always maintained within the metastable region where, given $\sigma(t)$, a unique solution for $T(t)$ in the domain of interest exists. Thus, for a given profile $\sigma(t)$, the temperature profile $T(t)$, which *realizes* $\sigma(t)$, is uniquely determined, depending on the initial conditions and the system dynamics.

3. OPTIMAL CONTROL

3.1 Problem formulation

In this section, we pose two optimal control problems emerging from the crystal shape manipulation task. To present the main ideas, we focus the discussion on the bidimensional crystal populations. The optimal control problem in higher dimensions and its solution remain conceptually the same, but the computation gets more extensive.

By considering $\sigma(t)$ as the control input to our system, we define the following optimal control problems

$$\textit{Problem 1':}\quad \min_{\sigma(t)\in[\underline{\sigma},\overline{\sigma}]} V_{C,\text{n}}(t_f) \quad \text{s.t.} \quad \begin{matrix}\ell_1(t_f)=\ell_{1,d}\\ \ell_2(t_f)=\ell_{2,d}\end{matrix} \tag{20}$$

$$\textit{Problem 2':}\quad \min_{\sigma(t)\in[\underline{\sigma},\overline{\sigma}]} V_{C,\text{n}}(t_f) \quad \text{s.t.} \quad \begin{matrix}\ell_1(t_f)=\ell_{1,d}\\ \ell_2(t_f)=\ell_{2,d}\\ t_f \le t_{f,c}\end{matrix} \tag{21}$$

For the input $\sigma(t)$, we accordingly define the upper and lower bounds, $\overline{\sigma}$ and $\underline{\sigma}$, respectively. The maximum limit is used to avoid primary nucleation, and is also motivated by the limitations on the temperature, while the minimum supersaturation limit is used to maintain the solution supersaturated. Note that we will allow $\underline{\sigma}$ to be chosen arbitrarily close [but not equal] to zero. *Problem 1'* reflects the basic shape manipulation problem of attaining a desired final shape for the seed crystals, while, in *Problem 2'*, additionally, the process is required to be completed within a fixed time interval $[0,t_{f,c}]$. In both cases, the amount (volume) of the resulting nucleation mass is penalized. It turns out that in contrast to the analogous optimal control problem for one-dimensional PBE (see Hofmann and Raisch [2010] and Bajcinca and Hofmann [2011]), the final time constraint may be *inactive*. This infers that for a given desired shape, the crystallization process under optimal control can never take longer than this limit.

3.2 Idealized model

The integro-differential model and the moment model, as defined by *Definition 1*, and *2*, respectively, are not appropriate for the application of the minimum principle, as this would lead to a two-point boundary value problem with relatively many unknown boundary values. Following a model simplification from Hofmann and Raisch [2010], where for one-dimensional processes, the natural feedback of the nucleation mass in the crystallization kinetics is entirely neglected, we introduce here a so-called *idealized model*, which will lead to an essentially simplified boundary value problem. More precisely, the idealization condition consists in adapting the equations (15a) and (15e) to

$$B(t) \approx k_b \sigma(t)^b V_{C,\text{s}}(t), \tag{22a}$$

$$c(t) \approx c_0 - \rho_c (V_{C,\text{s}}(t) - V_C(0)), \tag{22b}$$

where $V_{C,\text{s}}(t)$ is given by the polynomial expression (15g). This idealization is intuitively motivated by the optimal control problem itself, whose goal is the very minimization of the amount of nucleation. [To justify the idealization condition, and the acceptable accuracy of the resulting solution, it has to be verified that the feasible solution allows a "sufficiently low" minimal value for $V_{C,n}$.]

The integral expression for the net nucleation volume function $V_{c,\mathrm{n}}(t)$ given by

$$V_{C,\mathrm{n}}(t) = \int_0^t B(\xi)\eta\left(\ell_1(t) - \ell_1(\xi), \ell_2(t) - \ell_2(\xi)\right) d\xi \quad (23)$$

is intricate to use directly as a cost function. Therefore, following the approach in Bajcinca and Hofmann [2011], we introduce the modified integral expression

$$v_{C,\mathrm{n}}(t) = \int_0^t B(\xi)\eta\left(\ell_{1,d} - \ell_1(\xi), \ell_{2,d} - \ell_2(\xi)\right) d\xi \quad (24)$$

instead. Given that the equaltiy constraints $\ell_1(t_f) = \ell_{1,d}$ and $\ell_2(t_f) = \ell_{2,d}$ imply the condition $v_{C,\mathrm{n}}(t_f) = V_{C,\mathrm{n}}(t_f)$, and the fact that [due to the underlying idealization] $V_{C,\mathrm{n}}(t)$ does not affect the system solutions for all $t \in [0, t_f]$, a new model can be introduced, if (23) in the integro-differential model is substituted by (24). Such a model, referred to as the *idealized model*, then, reads:

Definition 3. (*Idealized ODE model).* Use $\sigma(t) > 0$ as input to compute $G_1(t)$, $G_2(t)$, $\ell_1(t)$, $\ell_2(t)$ and $V_{C,\mathrm{s}}(t)$, as before using (15b), (6) and (15g), respectively, whereas $B(t)$ is now computed using (22a). [The computation loop closes here.] The temperature $T(t)$, which is again a model output, is computed by solving the kinetics equations (15c), (15d) and the idealized mass-balance equation (22b) for $T(t)$. In addition, introduce, the state equation

$$\dot{v}_{C,\mathrm{n}} = B(t)\eta\left(\ell_{1,d} - \ell_1(t), \ell_{2,d} - \ell_2(t)\right), \; v_{C,\mathrm{n}}(0){=}0. \quad (25)$$

which, as indicated above, provides the value $V_{C,\mathrm{n}}(t_f)$ at $t = t_f$ [in accordance with the idealized $B(t)$ computed via (22a)], and therefore is suitable to use as a cost function.

3.3 Idealized model in τ-domain

Introduce a new "time" variable, τ, which is related to the "real" time t, via the ODE

$$\mathrm{d}\tau = G_1(t)\mathrm{d}t, \quad (26)$$

where $G_1(t) > 0$ is required for all $t \in [0, t_f]$. Choosing one of the growth rates as the time scaling function helps in simplifying the solution, as will be shown next. W.l.o.g. we assume for the exponential growth parameters $g_2 > g_1$, and $b > g_1$ and $b > g_2$. The latter two hold predominantly in practice, while for $g_1 > g_2$ define $\mathrm{d}\tau = G_2(t)\mathrm{d}t$.

In the transformed τ-domain, the idealized process kinetics becomes [the dependency on τ is designated by the '˜'-attribute]

$$\tilde{B}(\tau) = k_b\tilde{\sigma}(\tau)^b\tilde{V}_{C,s}(\tau), \quad (27a)$$

$$\tilde{G}_1(\tau) = k_{g_1}\tilde{\sigma}(\tau)^{g_1}, \;\; \tilde{G}_2(\tau) = k_{g_2}\tilde{\sigma}(\tau)^{g_2} \quad (27b)$$

$$\tilde{c}(\tau) = c_0 - \rho_c(\tilde{V}_{C,s}(\tau) - V_{C,s}(0)) \quad (27c)$$

and $\tilde{c}_{\mathrm{sat}}(\tau) = A_0 + A_1\tilde{T}(\tau) + A_2\tilde{T}(\tau)^2$. No state variable must be reserved for the evolution of $\tilde{\ell}_1(\tau)$, as $\tilde{\ell}_1(\tau) = \tau$. By introducing the state variables

$$x_1 \triangleq \tilde{\ell}_2, \;\; x_2 \triangleq \tilde{v}_{C,n}, \;\; x_3 \triangleq \tilde{t} \quad (27d)$$

we, effectively, retain the following ODE system that will be utilized to solve the optimal control problem

$$\frac{\mathrm{d}x_1}{\mathrm{d}\tau} = \frac{k_{g_2}}{k_{g_1}}\tilde{\sigma}^{g_2-g_1} \quad (27e)$$

$$\frac{\mathrm{d}x_2}{\mathrm{d}\tau} = \frac{k_b}{k_{g_1}}\tilde{\sigma}^{b-g_1}\tilde{V}_{C,s}(\tau, x_2)\tilde{\eta}\left(\ell_{1,d} - \tau, \ell_{2,d} - x_1\right) \quad (27f)$$

$$\frac{\mathrm{d}x_3}{\mathrm{d}\tau} = \frac{1}{k_{g_1}}\tilde{\sigma}^{-g_1}, \quad (27g)$$

with zero initial conditions. Note that the time $\tilde{t}$ appears as an additional state due to the time-constraint in the optimal control in *Problem 2*, and for back-transformation of the optimal solution to the t-domain, a step which has to be carried out ultimately for its implementation to a real process. Moreover, using $\tilde{\ell}_1(\tau) = \tau$, (15g) simplifies to

$$\begin{aligned}\tilde{V}_{C,s}(\tau) = &\left(\tfrac{1}{3}\tau^3 + \left(\tilde{\ell}_2(\tau) - \tau\right)\tau^2\right)\mu_{00}(0)\\ &+ 2\tau\left(\tilde{\ell}_2(\tau) - \tau\right)\mu_{10}(0) + \left(\tilde{\ell}_2(\tau) - 2\tau\right)\mu_{2,0}(0)\\ &+ \tau^2\mu_{0,1}(0) + 2\tau\mu_{1,1}(0) + V_{C,s}(0). \quad (28)\end{aligned}$$

The optimal control problems in the idealized and time scaled model now read

$$\textit{Problem 1:} \quad \min_{\tilde{\sigma}(\tau)\in[\underline{\sigma},\overline{\sigma}]} \tilde{v}_{C,n}(\tau_f) \quad \text{s.t.} \quad \begin{matrix}\tau_f = \ell_{1,d}\\ \tilde{\ell}_2(\tau_f) = \ell_{2,d}\end{matrix} \quad (29)$$

$$\textit{Problem 2:} \quad \min_{\tilde{\sigma}(\tau)\in[\underline{\sigma},\overline{\sigma}]} \tilde{v}_{C,n}(\tau_f) \quad \text{s.t.} \quad \begin{matrix}\tau_f = \ell_{1,d}\\ \tilde{\ell}_2(\tau_f) = \ell_{2,d}\\ \tilde{t}(\tau_f) \le t_{f,c}\end{matrix} \quad (30)$$

Note that compared to *Problem 1'*, *Problem 1* is simplified in the τ-domain, as the model order is reduced by one [due to $\ell_1 = \tau$], and, the final "time" τ_f is now fixed.

3.4 Minimum principle solutions

The idealized ODE model in the τ-domain with the states $\mathbf{x} = [x_1, x_2, x_3]^T$, including the simplified kinetics (27a)-(27g), is suitable apply the minimum principle. The Hamiltonian $\mathcal{H}$, and the adjoint system with the costates $\Psi = [\psi_1, \psi_2, \psi_3]^T$ is the same for both optimal control problems, while the necessary conditions required by the minimum principle differ only in the boundary conditions. The Hamiltonian $\mathcal{H} = \Psi^T\frac{\mathrm{d}}{\mathrm{d}\tau}\mathbf{x}$ reads

$$\begin{aligned}\mathcal{H}\left(\mathbf{x}, \Psi, \tilde{\sigma}, \tau\right) = &\psi_1\frac{k_{g_2}}{k_{g_1}}\tilde{\sigma}^{g_2-g_1} + \psi_2\frac{k_b}{k_{g_1}}\tilde{\sigma}^{b-g_1}\times\\ &\times\tilde{V}_{C,s}(\tau, x_1)\eta\left(\ell_{1,d} - \tau, \ell_{2,d} - x_1\right) + \psi_3\frac{1}{k_{g_1}}\tilde{\sigma}^{-g_1}, \quad (31a)\end{aligned}$$

with the adjoint system given by

$$\begin{aligned}\tfrac{\mathrm{d}}{\mathrm{d}\tau}\psi_1 = &-\psi_2\frac{k_b}{k_{g_1}}\tilde{\sigma}^{b-g_1}\times\\ &\times\frac{\partial}{\partial x_1}\left[\tilde{V}_{C,s}(\tau, x_1)\eta\left(\ell_{1,d} - \tau, \ell_{2,d} - x_1\right)\right], \quad (31b)\end{aligned}$$

$$\tfrac{\mathrm{d}}{\mathrm{d}\tau}\psi_2 = 0, \quad (31c)$$

$$\tfrac{\mathrm{d}}{\mathrm{d}\tau}\psi_3 = 0. \quad (31d)$$

Solution to Problem 1: According to the minimum principle, in this case, the boundary conditions for each state and costate, corresponding to the optimal solutions (always denoted by a '*'), are simple

$$x_1^*(0) = 0; \qquad x_2^*(0) = 0; \qquad x_3^*(0) = 0; \quad (32a)$$

$$x_1^*(\tau_f) = \ell_{2,d}; \qquad \psi_2^*(\tau_f) = 1; \qquad \psi_3^*(\tau_f) = 0. \quad (32b)$$

In addition, the final "time" τ_f is fixed and known

$$\tau_f = \ell_{1,d}. \quad (32c)$$

It immediately follows that

$$\psi_2^*(\tau) = 1, \;\; \forall\tau \in [0, \tau_f] \quad (32d)$$

$$\psi_3^*(\tau) = 0, \;\; \forall\tau \in [0, \tau_f]\,. \quad (32e)$$

At each "time" instant $\tau \in [0, \tau_f]$, the optimal control input, $\tilde{\sigma}^*(\tau)$, must globally minimize $\mathcal{H}$, hence

$$\tilde{\sigma}^*(\tau) = \underset{\tilde{\sigma}\in[\underline{\sigma},\overline{\sigma}]}{\operatorname{argmin}} \mathcal{H}\left(\mathbf{x}^*, \Psi^*, \tilde{\sigma}, \tau\right)$$
$$= \underset{\tilde{\sigma}\in[\underline{\sigma},\overline{\sigma}]}{\operatorname{argmin}} \Big(\psi_1^* \frac{k_{g_2}}{k_{g_1}} \tilde{\sigma}^{g_2-g_1} + \psi_2^* \frac{k_b}{k_{g_1}} \tilde{\sigma}^{b-g_1} \times$$
$$\times \tilde{V}_{C,s}(\tau, x_1^*) \eta\left(\ell_{1,d} - \tau, \ell_{2,d} - x_1^*\right) \Big). \quad (32f)$$

A candidate for $\tilde{\sigma}^*(\tau)$ is a solution $\tilde{\sigma}^o(\tau) \in [\underline{\sigma}, \overline{\sigma}]$, defined by $\frac{\partial}{\partial\tilde{\sigma}}\mathcal{H} = 0$, which is given by

$$\tilde{\sigma}^o(\tau) = \Bigg(-\frac{1}{\psi_1}\frac{k_b}{k_{g_2}}\frac{b-g_1}{g_2-g_1} \tilde{V}_{C,s}\left(\tau, x_1^*\right) \times$$
$$\times \eta\left(\ell_{1,d} - \tau, \ell_{2,d} - x_1^*\right) \Bigg)^{-\frac{1}{b-g_2}}, \quad (32g)$$

provided that $\psi_1^*(\tau) < 0$. Otherwise, $\tilde{\sigma}^*(\tau) = \underline{\sigma}$, as both summation terms in (32f) are positive and $b > g_2 > g_1$. Therefore, the optimal control can be declared by

$$\tilde{\sigma}^*(\tau) = \underset{\tilde{\sigma}\in\{\underline{\sigma}, \tilde{\sigma}^o, \overline{\sigma}\}}{\operatorname{argmin}} \mathcal{H}\left(\mathbf{x}^*, \Psi^*, \tilde{\sigma}, \tau\right). \quad (32h)$$

The problem of finding the optimal control has been reduced to a two-point boundary value problem, which can be solved by finding the only unknown initial condition $\psi_1^*(0)$.

Solution to Problem 2: To deal with the additional inequality constraint, $x_3(\tau_f) \leq t_{f,c}$, one needs to know, whether the constraint is active or not. For instance, in a first step, the optimal control *Problem 1* is solved. If $x_3^*(\tau_f) < t_{f,c}$ results, then the underlying solution is also a solution to *Problem 2*, since the time constraint is not active. In all other cases, one can replace the inequality constraint by the equality one $x_3(\tau_f) = t_{f,c}$. This leads to the following boundary conditions

$$x_1^*(0) = 0; \qquad x_2^*(0) = 0; \qquad x_3^*(0) = 0; \quad (33a)$$
$$x_1^*(\tau_f) = \ell_{2,d}; \qquad \psi_2^*(\tau_f) = 1; \qquad x_3^*(\tau_f) = t_{f,c}. \quad (33b)$$

Again, the final "time" τ_f is fixed and known

$$\tau_f = \ell_{1,d}. \quad (33c)$$

At each "time" instant $\tau \in [0, \tau_f]$, the optimal control input, $\tilde{\sigma}^*(\tau)$, must globally minimize $\mathcal{H}$

$$\tilde{\sigma}^*(\tau) = \underset{\tilde{\sigma}\in[\underline{\sigma},\overline{\sigma}]}{\operatorname{argmin}} \mathcal{H}\left(\mathbf{x}^*, \Psi^*, \tilde{\sigma}, \tau\right)$$
$$= \underset{\tilde{\sigma}\in[\underline{\sigma},\overline{\sigma}]}{\operatorname{argmin}} \Big(\psi_1^* \frac{k_{g_2}}{k_{g_1}} \tilde{\sigma}^{g_2-g_1} + \psi_2^* \frac{k_b}{k_{g_1}} \tilde{\sigma}^{b-g_1} \times$$
$$\times \tilde{V}_{C,s}(\tau, x_1^*) \eta\left(\ell_{1,d} - \tau, \ell_{2,d} - x_1^*\right) + \psi_3^* \frac{1}{k_{g_1}} \tilde{\sigma}^{-g_1} \Big) \quad (34)$$

Note that $\psi_3^* = \text{const}$ must be a positive constant, $\psi_3^* > 0$, otherwise, [that is, if $\psi_3^* < 0$] due to the last term in (34) [which becomes dominant for small $\tilde{\sigma}$], and if $\underline{\sigma}$ is chosen small enough, $\tilde{\sigma}^*(\tau) = \underline{\sigma}$, $\forall\tau \in [0, \tau_f]$ would hold, and the time-constraint would be violated.

In this case, $\frac{\partial}{\partial\tilde{\sigma}}\mathcal{H} = 0$ can not be solved analytically. Instead, the following equation has to be solved numerically for $\tilde{\sigma}^o(\tau)$ [again, we drop the implicit dependencies on τ]

$$k_b(b-g_1)(\tilde{\sigma}^o)^b \tilde{V}_{C,s}(\tau, x_1^*)\eta(\ell_{1,d} - \tau, \ell_{2,d} - x_1^*)$$
$$+ \psi_1^* k_{g_2}(g_2 - g_1)(\tilde{\sigma}^o)^{g_2} - \psi_3^* g_1 = 0.$$

The optimal control problem is therefore reduced to a two-point boundary value problem, involving two unknown initial conditions $\psi_1^*(0)$ and $\psi_3^* = \text{const}$. For its solution, *e.g.* a single shooting numerical method can be used (see Section 4).

Implementation in the t-domain: The computed optimal solution $\tilde{\sigma}^*(\tau)$ refers to the idealized model given by *Definition 3*. It does not identically match to the optimal profile of the exact integro-differential model (*Definition 1*) or moment model (*Definition 2*). This section concerns the errors, resulting from the use of the underlying idealization conditions (22a)-(22b). Here, we construct a feasible sub-optimal temperature profile in the "real" time domain, denoted by $\hat{T}(t)$, which guarantees the constraints, and provides an upper bound for the minimal possible cost. Related thorough discussions can be found in Hofmann and Raisch [2010] and Bajcinca and Hofmann [2011].

For the implementation of the solution $\tilde{\sigma}^*(\tau)$ to the optimal control problems with free or constrained t_f, two final steps have to be carried out, additionally. First, the signals, in particular $\tilde{\sigma}^*(\tau)$, must be back-transformed to the "normal" time t-domain. Therefore, the inverse function [denoted by $\tau^*(t)$] of the optimal time trajectory $t = x_3^*(\tau)$, representing the optimal profile of the variable τ in the t-domain, is to be used in accordance with

$$\sigma^*(t) = \tilde{\sigma}^*\left(\tau^*(t)\right), \quad t \in [0, x_3^*(\tau_f)]. \quad (35)$$

To compute the temperature profile in the t-domain, which is ultimately needed as the input to a crystallization process in practice, one could apply the available profile $\sigma^*(t)$ as the input to the idealized model from *Definition 3*. The temperature profile resulting from this, however, is not preferable for application to a real process, as it would very likely lead to the constraints violation. On the other hand, if $\sigma^*(t)$ is used as the input to the integro-differential model (*Definition 1*) or moment model (*Definition 2*), it is obvious that the constraints $\ell_1(t_f) = \ell_{1,d}$ and $\ell_2(t_f) = \ell_{2,d}$ defined by the final desired morphology of the underlying crystal population, in addition to the time constraint in *Problem 2* are precisely held. This is a consequence of the fact, that the idealization conditions (22a)-(22b) do not affect the trajectory $(\ell_1(t), \ell_2(t))$ in (6) [with σ defined as the input]. Hence, if the resulting temperature profile $\hat{T}(t)$ would be applied to the real process, the supersaturation profile $\sigma^*(t)$ is, per construction realized, and therefore the constraints must hold, too.

To summarize, we suggest such constructed temperature profiles $\hat{T}(t)$, $t \in [0, t_f]$, as convenient sub-optimal solutions to the original optimal control problems *Problem 1'* and *Problem 2'*. Note that this is a feasible solution, in that it guarantees all constraints, and therefore, provides an upper bound for the cost in *Problem 1'* and *Problem 2'*.

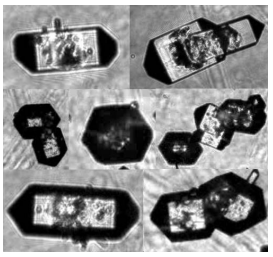

(a)

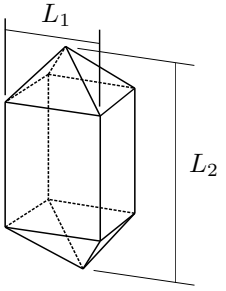

(b)

Fig. 2. KDP crystals.

4. NUMERICAL EXAMPLE

A numerical example for illustrating the proposed optimal control algorithm for shape manipulation of a bidimensional crytal population is extensively discussed in this

section. As a case study we consider potassium dihydrogen phosphate (KH_2PO_4, abbr. KDP), see Fig. 2. The model parameters are listed in Table 2. The initial seed distribution $f_{\text{seed}}(L_1, L_2)$ is adapted from Ma et al. [2002] to satisfy the geometrical condition $L_2 > L_1$ for all particles of the population, and is given by

$$f_{\text{seed}} = -6.99\times10^{-4}(L_1^2+L_2^2)+0.25L_1+0.33\,L_2-65.52$$

for $L_1 \in [160, 220]$, $L_2 \in [220, 280]$ (in [μm] units), and null otherwise. The intial seed mass is 5.6 [mg]. Note that f_{seed} is parabola-like shaped, centered at $(196, 256)$ [μm]. The desired center for the seed PDF at the end of the batch is $(320, 630)$ [μm], which provides the equality optimization constraints at $(\ell_{1,d}, \ell_{2,d}) = (124, 374)$ [μm]. In *Problem 2'* resp. *Problem 2*, the final time constraint is set to two hours, $t_{f,c} = 7200$ [s]. The supersaturation is limited by $\underline{\sigma} = 0.1\%$ and $\overline{\sigma} = 6\%$.

The single shooting method is used to solve the two-point boundary value problems, resulting from the application of the minimum principle to *Problem 1* and *Problem 2*, as defined in Section 3.3. For *Problem 1*, where the final time t_f is free, the boundary value problem involves the initial value $\psi_1^*(0)$, as the only unknown parameter, which is determined by using the `fzero` function from Matlab®, in conjunction with the `ode15s` solver. If the final time constraint $t_f \leq t_{f,c}$ is active, the solution to *Problem 2* is more demanding, as the initial values of two costates, namely, $\psi_1^*(0)$ and $\psi_3^*(0)$, are unknown. Therefore, the solver `bvp4c` of Matlab® is employed.

For comparison purposes, the optimal control problems *Problem 1* and *Problem 2* are solved also with a dynamic optimization approach using the `fmincon` non-linear programming tool from Matlab®. Thereby, the control profile $\tilde{\sigma}(\tau)$ is discretized using a uniform grid with a spacing equal to 2 [μm] in the interval $[0, \ell_{1,d}]$, while a first-order interpolation between the grids is applied.

In Table 1 we provide some important outcomes obtained by making use of the minimum principle (PMP), and the dynamic optimization (DYN), for the two underlying optimization scenarios *Problem 1* and *Problem 2*. Note that the signs of the resulting costate initial values $\psi_1^*(0) < 0$ and $\psi_3^*(0) > 0$ are in agreement with the discussion in Section 3.4. The very good matching between the outcomes corresponding to the minimum principle and the dynamic optimization solutions is a strong indicator for their correctness. Furthermore, as intuitively expected, the cost $v_{C,\text{n}}^*(t_f)$ in *Problem 2* must increase due to the introduced final time constraint of 2 [h]. Additionally, in the table is included $\hat{V}_{C,\text{n}}(t_f)$, which results from the simulation of the non-idealized models from *Definition 1* or *Definition 2* with $\sigma^*(t)$ as input. As discussed in the previous section, this represents an upper bound for the cost in the real process under optimal control.

Table 1.

	Problem 1		*Problem 2*	
	PMP	DYN	PMP	DYN
$\psi_1^*(0)$ ($\times10^6$)	-2.55		-0.992	
$\psi_3^*(0)$ ($\times10^3$ [μm^3/s])			8.611	
$v_{C,\text{n}}^*(t_f)$ ($\times10^6$ [μm^3])	300.873	300.875	324.436	324.431
$\hat{V}_{C,\text{n}}(t_f)$ ($\times10^6$ [μm^3])	303.800	308.234	325.437	329.248
t_f^* [h]	6.627	6.621	2	2
computation time [s]	4.99	29.33	188	32

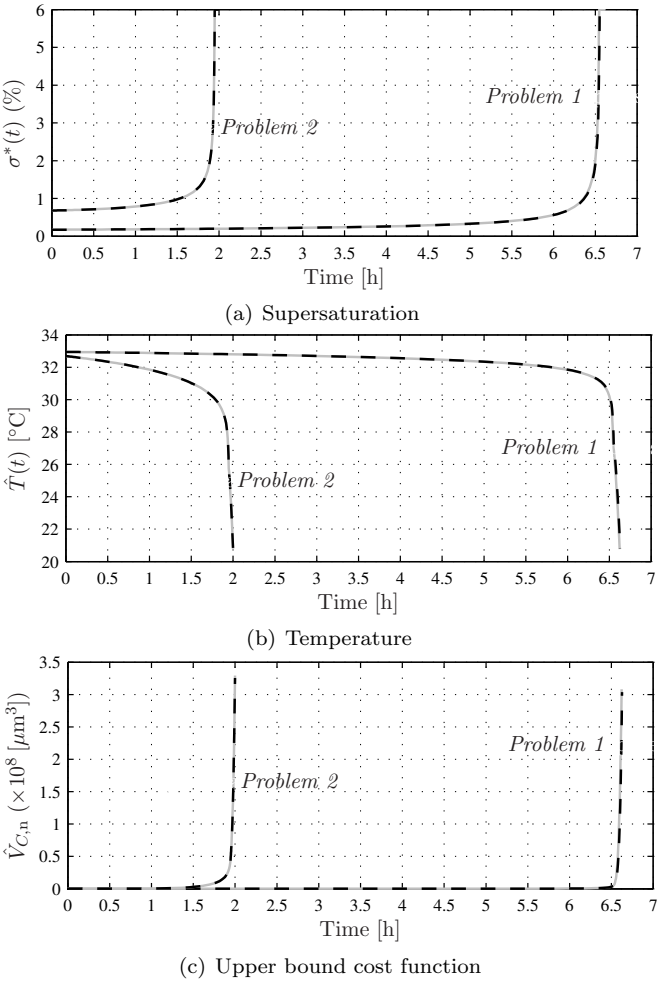

(a) Supersaturation

(b) Temperature

(c) Upper bound cost function

Fig. 3. Optimal solutions for *Problem 1* and *Problem 2* (black lines refer to PMP; gray to DYN).

In Fig. 3 we depict the evolution of the optimal supersaturation profile $\sigma^*(t)$, the sub-optimal temperature profile $\hat{T}(t)$ (see Section 3.4.3), and the corresponding net volume of nucleated crystals $\hat{V}_{C,\text{n}}(t)$, respectively. Note that the temperature and supersaturation plots exhibit a typical behavior, which is well known in optimal control of batch crystallization. Namely, a flat part prevailing for most of the time is followed by a steep decrease of the temperature corresponding to a steep increase of supersaturation, shortly before the process is completed. From Fig. 3(a) one can observe that the supersaturation referring to *Problem 2*, must be kept at a higher level in order to complete the shape manipulation task in a shorter time. Also, in the solutions to both *Problem 1* and *Problem 2* the supersaturation constraint $\underline{\sigma}$ is always inactive, indicating that $\psi_1^*(t) < 0$ for all $t \in [0, t_f]$ [recall the discussion in Section 3.4]. All plots indicate a very tight match in the trajectories of the optimal solutions, resulting from the application of the minimum principle and dynamic optimization.

Finally, for validation purposes, the PDF $f(L_1, L_2, t_f)$ can be reconstructed using the evolution of the moments computed via the model in *Definition 2*. Therefore, we utilized the method suggested in Qamar and Seidel-Morgenstern [2009]. The results are depicted in Fig. 4 and Fig. 5, referring to *Problem 1'* with free time duration, and

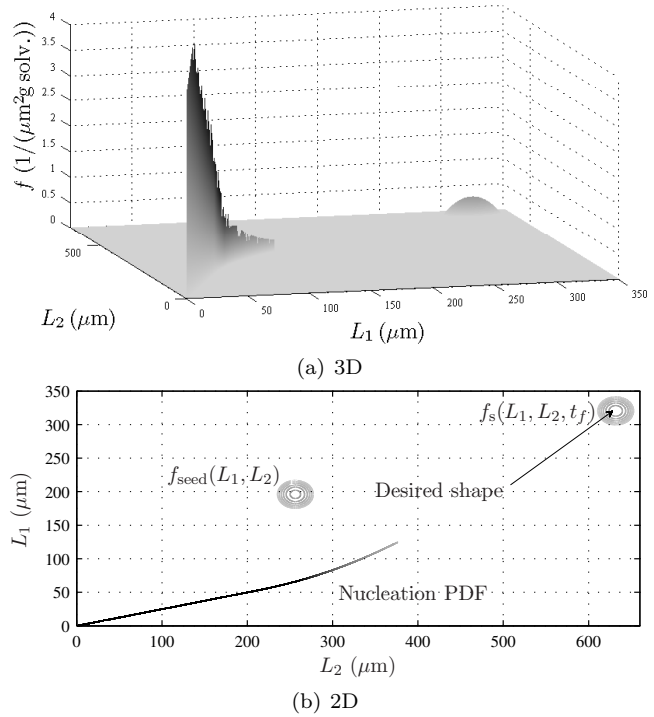

(a) 3D

(b) 2D

Fig. 4. Evolution of the optimal PDF for *Problem 1.*

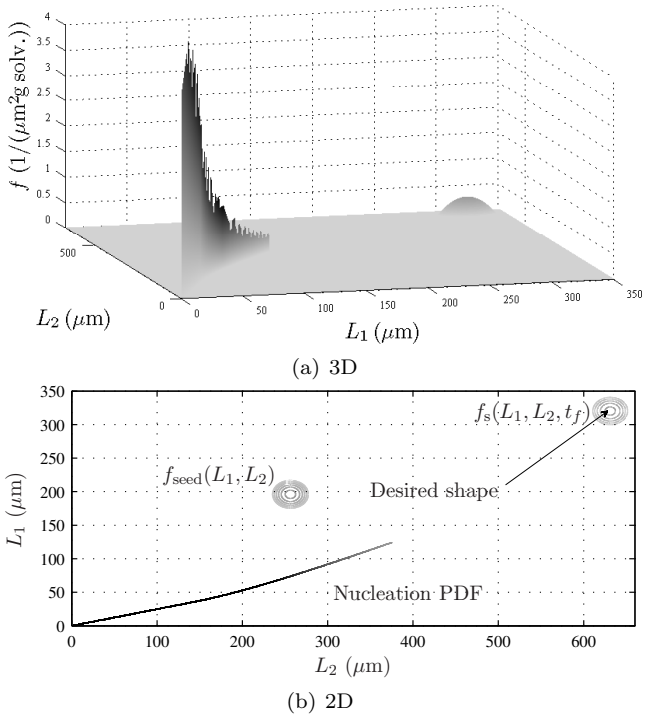

(a) 3D

(b) 2D

Fig. 5. Evolution of the optimal PDF for *Problem 2.*

Problem 2' with limited time duration, respectively. Both figures indicate that the obtained size and shape for the seed crystals fit very well to the desired one. Note also, that the state-space constraints $L_2 > L_1$ [which we did not explicitly consider!], defined by the morphology of the KDP crystals are not violated.

5. CONCLUSION

Optimal control problem for crystal shape manipulation of a multidimensional population of crystal particles has been addressed. The general goal in attaining a population of crystals with a desired morphology, naturally leads to an optimal control problem, where seed crystals must be grown towards a prespecified shape, while the overall mass of nucleated particles is to be minimized. Using the method of characteristics and a physically motivated simplifying condition, we derive a closed ODE system, which is suitable for the application of the minimum principle. We present solutions to optimal control problems, either with or without a limitation on the process duration, which essentially reduce to boundary value problems, involving only one or two unknown variables. In addition, for the original problem setting, including the full process dynamics, a simple feasible sub-optimal solution and an upper bound for the cost function are proposed.

Table 2.

Parameter	Value	Units
k_{g_1}	12.1	μm×s^{-1}
k_{g_2}	100.75	μm×s^{-1}
k_b	7.49×10^{-8}	# μm^{-3}×s^{-1}
g_1	1.48	—
g_2	1.74	—
b	2.04	—
A_0	0.21	g/g solv.
A_1	-9.76×10^{-5}	g×°C^{-1} /g solv.
A_2	9.30×10^{-5}	g×°C^{-2} /g solv.
c_0	0.31	g/g solv.
ρ_c	2.34×10^{-12}	g×μm^{-3}

REFERENCES

Ajinkya, M. and Ray, W. (1974). On the optimal operation of crystallization processes. *Chem. Eng. Commun.*, 1, 181–186.

Bajcinca, N. and Hofmann, S. (2011). Optimal control for batch crystallization with size-dependent growth kinetics. *American Control Conference 2011, San Francisco, USA.*

Bajcinca, N., Oliveira, V., Borchert, C., Raisch, J., and Sundmacher, K. (2010). Optimal control solutions for crystal shape manipulation. 874–885.

Bajcinca, N., Perl, R., and Sundacher, K. (2011). Convex optimization for shape manipulation of multidimensional crystal particles.

Braatz, R. and Hasebe, S. (2002). Particle size and shape control in crystallization processes. *AIChE Symposium Series*, 98(326).

Charpentier, J.C. (2009). Perspective on multiscale methodology for product design and engineering. 33, 936–946.

Hofmann, S. and Raisch, J. (2010). Application of optimal control theory to a batch crystallizer using orbital flatness.

Jones, A. (1974). Optimal operation of a batch cooling crystallizer. *Chem. Eng. Sci.*, 29, 1075–1087.

Lang, Y., A.M.Cervantes, and Biegler, L. (1999). Dynamic optimization of a batch cooling crystallization process. *Ind. Eng. Chem. Res.*, 38(4), 1469–1477.

Ma, D., Tafti, D., and Braatz, R. (2002). Optimal control and simulation of multidimensional crystallization processes. *Computers and Chemical Engineering*, 26, 1103–1116.

Miller, S. and Rawlings, J. (1994). Model identification and control strategies for batch cooling crystallizers. *International Journal of Control*, 40, 1312–1327.

Mullin, J.W. and Nyvlt, J. (1971). Programmed cooling of batch crystallizers. *CES*, 26(3), 369–377.

Patience, D. and Rawlings, J. (2001). Particle-shape monitoring and control in crystallization processes. *AIChE*, 47(9), 2125–2130.

Qamar, S. and Seidel-Morgenstern, A. (2009). An efficient numerical technique for solving multi-dimensional batch crystallization models with size independent growth rates. *Computers & Chemical Engineering*, 33(7), 1221–1226.

Yang, H.G., Sun, C.H., Qiao, S.Z., Zou, J., L.G., Smith, S.C., M., C.H., and Lu, G.Q. (2008). Anatase tio2 single crystals with a large percentage of reactive facets. 453, 638–642.